Characterization of Gd loaded chitosan-TPP nanohydrogels by a multi-technique approach combining dynamic light scattering (DLS), asymetrical flow-field-flow-fractionation (AF4) and atomic force microscopy (AFM) and design of positive contrast agents for molecular

2017 Nanotechnology 28 055705

(http://iopscience.iop.org/0957-4484/28/5/055705)

IOP Publishing Nanotechnology
Nanotechnology 28 (2017) 055705 (15pp) doi:10.1088/1361-6528/aa5188

Characterization of Gd loaded chitosan-TPP nanohydrogels by a multi-technique approach combining dynamic light scattering (DLS), asymetrical flow-field-flow-fractionation (AF4) and atomic force microscopy (AFM) and design of positive contrast agents for molecular resonance imaging (MRI)

G Rigaux[1], C V Gheran[2], M Callewaert[1,9], C Cadiou[1], S N Voicu[2,3], A Dinischiotu[2], M C Andry[1], L Vander Elst[4,5], S Laurent[4,5], R N Muller[4,5], A Berquand[6], M Molinari[6], S Huclier-Markai[7,8] and F Chuburu[1,9]

[1] Institut de Chimie Moléculaire de Reims, CNRS UMR 7312, Université de Reims Champagne-Ardenne URCA, F-51685 Reims Cedex 2, France
[2] Faculty of Biology, Department of Biochemistry and Molecular Biology, University of Bucharest, Bucharest, Romania
[3] Faculty of Pharmacy, Department of Pharmacy, Titu Maiorescu University, Bucharest, Romania
[4] Laboratoire de RMN et d'Imagerie Moléculaire, Université de Mons, B-7000 Mons, Belgique
[5] Center for Microscopy and Molecular Imaging, Rue Adrienne Bolland 8, B-6041 Charleroi, Belgium
[6] Laboratoire de Recherche en Nanosciences—EA 4682, Plate-forme Nano'Mat, Université de Reims Champagne-Ardenne URCA, F-51685 Reims Cedex 2, France
[7] Laboratoire Subatech, UMR 6457, Ecole des Mines de Nantes/CNRS/IN2P3/Université de Nantes, 4 Rue A. Kastler, BP 20722, F-44307 Nantes Cedex 3, France
[8] ARRONAX GIP, 1 rue Arronax, F-44817 Nantes Cedex, France

E-mail: maite.callewaert@univ-reims.fr and francoise.chuburu@univ-reims.fr

Received 26 September 2016, revised 28 November 2016
Accepted for publication 5 December 2016
Published 28 December 2016

Abstract

Chitosan CS—tripolyphosphate TPP/hyaluronic acid HA nanohydrogels loaded with gadolinium chelates (GdDOTA ⊂ CS-TPP/HA NGs) synthesized by ionic gelation were designed for lymph node (LN) MRI. In order to be efficiently drained to LNs, nanogels (NGs) needed to exhibit a diameter $\phi < 100$ nm. For that, formulation parameters were tuned, using (i) CS of two different molecular weights (51 and 37 kDa) and (ii) variable CS/TPP ratio ($2 <$ CS/TPP < 8). Characterization of NG size distribution by dynamic light scattering (DLS) and asymetrical flow-field-flow-fractionation (AF4) showed discrepancies since DLS diameters were consistently above 200 nm while AF4 showed individual nano-objects with $\phi < 100$ nm. Such a difference could be correlated to the presence of aggregates inherent to ionic gelation. This point was clarified by atomic force

[9] Author to whom any correspondence should be addressed.

microscopy (AFM) in liquid mode which highlighted the main presence of individual nano-objects in nanosuspensions. Thus, combination of DLS, AF4 and AFM provided a more precise characterization of GdDOTA ⊂ CS-TPP/HA nanohydrogels which, in turn, allowed to select formulations leading to NGs of suitable mean sizes showing good MRI efficiency and negligible toxicity.

Keywords: nanohydrogels, chitosan, DLS, AF4, AFM-PFQNM, MRI contrast agents

(Some figures may appear in colour only in the online journal)

Introduction

Given its great 3D spatial resolution and its unlimited tissue penetration, magnetic resonance imaging (MRI) is one of the most powerful diagnostic techniques in clinical medicine. It can, in a non-invasive way and without the use of ionizing radiation, differentiate pathological tissues from normal ones on the basis of fluctuations of longitudinal (T_1) and transversal (T_2) proton relaxation times of water protons [1]. Indeed, with respect to normal areas, in pathological tissues T_1 and T_2 relaxation times may be altered and these differences can be converted into images [1, 2]. One of the major challenges in MRI is sensitivity. Actually, information obtained from a simple unenhanced MR image is often not sufficient to highlight the areas of interest. Thus the contrast has to be improved and for that, paramagnetic complexes of metal ions such as gadolinium chelates (GdCAs) are frequently used. GdCAs catalyze the longitudinal ^{1}H relaxation process of surrounding water protons [1–4]. Change in longitudinal relaxation results in a signal intensity increase (positive contrast) of most abnormal tissues which facilitates visualization of lesions. For a Gd chelate, the efficiency to reduce proton T_1 relaxation time is defined by its longitudinal relaxivity r_1 which represents the enhancement of the relaxation rate ($1/T_1$) referred to a 1 mM concentration of the GdCA. For commercially available GdCAs, r_1 stands in the range 3–5 s^{-1} mM^{-1} at 60 MHz, which is rather low. To increase current GdCAs efficacy Solomon–Bloembergen–Morgan (SBM) theory [5] provides guidelines which are mainly based on the slow-down of GdCAs tumbling motion and on optimization of water residence times in the gadolinium coordination sphere. One approach consists in grafting GdCAs on macromolecules and nanoparticles [6, 7] in order to increase the so-called rotational correlation time of the chelates. These approaches although extremely useful failed to reach the maximum in relaxivity predicted by the SBM theory (100 mM^{-1} s^{-1} in 20–60 MHz range [1–3]). Recently, strategies based on spatial confinement of GdCAs within nano-objects have appeared [8–13]. They allowed to reach this milestone since longitudinal relaxivity r_1 higher than 100 mM^{-1} s^{-1} at 60 MHz per Gd^{3+} ion were obtained. Obviously, these hypersensitive T_1 MRI probes are of particular interest to improve MRI sensitivity in clinical applications, provided they are biocompatible. Hydrogels constituted a novel class of three-dimensional hydrophilic cross-linked polymers that display unique properties such as drug-loading capacity and water-retention ability [14]. In that sense they can be very useful for the spatial confinement of GdCAs and the development of hypersensitive T_1 MRI probes. Recently, we have demonstrated that nanohydrogels can be used to encapsulate GdCAs (such as GdDOTA, GdDOTP and MS325) [15, 16]. Nanohydrogels were obtained by ionic gelation of chitosan (CS) and sodium hyaluronate (HA), two natural polysaccharides. CS is composed of N-acetylglucosamine and glucosamine residues [17, 18] while HA consists of a linear chain of fragments of D-glucuronic acid and N-acetyl-glucosamine [19, 20]. HA is ubiquitous in the human body and is involved in many cellular functions such as water homeostasis. By exploiting polycationic nature of CS and polyanionic nature of HA we have prepared nanohydrogels (NGs), under mild conditions and without the use of solvents except water, for which stability was improved by ionic cross-linking with sodium tripolyphosphate (TPP). These NPs of mean diameters comprised between 150 and 280 nm are able to confine important amounts of GdCAs (up to 50 mM of GdCAs inside NGs [15]). The so-designated GdCA ⊂ NGs observed SBM theory requirements (restricted rotational motions of confined GdCA and water permeability of the matrix) and allowed to reach high r_1 values around 100 mM^{-1} s^{-1} per Gd^{3+} ion (37 °C and 20 MHz). Furthermore they elicit both T_1 and T_2 responses which represent a real advance to better differentiate between normal and pathological tissues. GdCA ⊂ NGs could therefore be useful in MR imaging to detect the presence of metastases in lymph nodes. The lymphatic system is an essential element of the immune system and, in many cancers, a major route for dissemination of metastatic cancer cells. The pre-therapeutic detection of metastases in lymph nodes is therefore crucial to determining prognosis and appropriate treatment [21]. In order to image in one injection a large number of lymph nodes, it is recommended to administer a lymphographic contrast agent by intravenous injection. For an efficient lymphatic drainage, the required nanoparticle size is in the range 50–100 nm [22]. It is then necessary to decrease the current GdCA ⊂ NGs mean sizes. It was recently demonstrated that CS molecular weight influenced NG morphology in such a way that GdCA ⊂ NGs larger CS molecular weight led to larger NPs [23]. The ionic gelation method has also the advantage to allow the adjustement of NG sizes by the variation of parameters such CS/TPP ratios [24–26].

With these data in mind, we have re-investigated gadolinium nanohydrogel syntheses and compared NG morphologies obtained with two CS of 51 and 37 kDa respectively, under different CS/TPP ratios. For that, GdDOTA which corresponds to the active substance of DOTAREM® was

considered as GdCA [15]. From a methodological point of view, GdDOTA ⊂ CS-TPP/HA NG morphologies were analyzed by means of dynamic light scattering (DLS), asymmetrical flow-field-flow-fractionation (AF4) and atomic force microscopy (AFM), in order to have a reliable characterization of the nanosuspensions in terms of NP size and density. Those hyphenated techniques allowed to select GdDOTA ⊂ CS-TPP/HA NGs of mean diameters suitable for injection. The influences of CS molecular weight and CS/TPP ratios on GdDOTA loadings were also studied. The potential *in vivo* efficacy of relevant GdDOTA ⊂ CS-TPP/HA NGs was then investigated by relaxivity measurements of the nanosuspensions, for which safety was assured by viability, cytotoxicity and oxidative stress assays on endothelial murine cells (SVEC-10 cells).

Method section

General

Chitosan CS51 (51 kDa, low viscosity, from shrimp shells, 86% deacetylated) and sodium hyaluronate (1000 kDa extracted from *Streptococcus equi sp*) were purchased from Sigma (France). KiOmedine® ultrapure chitosan CS37 of non-animal origin, with an ultra-low molecular weight of 37 kDa (average viscosity molecular weight determined by capillary viscosimetry) and a deacetylation degree of 90% (determined by ^{1}H NMR, 500 MHz, 318 K, 1 μl DCl/700 μl D_2O) obtained from KiOmed Pharma (Belgium). Sodium tripolyphosphate (TPP) was purchased from Acros Organics. All products were used as received without further purification. HGdDOTA was synthesized according to a previously published procedure [15]. Sterile water for injection (Laboratoire Aguettant, Lyon, France) was systematically used for nanoparticle preparation and analysis. Fetal bovine serum and Dulbecco's Modified Eagle Medium were purchased from Gibco (USA) and WesternBreeze® Chromogenic *Kits* were procured from Invitrogen (Carlsbad, CA, USA). Antibiotic antimycotic solution stabilized with 10.000 units penicillin, 10 mg streptomycin and 25 μg amphotericin B per ml, *In Vitro* Toxicology Assay Kit Sulforhodamine B based, *In Vitro* Toxicology Assay Kit Lactic Dehydrogenase based, reduced glutathione (GSH), 5,5-dithio-bis-(2-nitrobenzoic acid), thiobarbituric acid and 1, 1, 3, 3-tetramethoxypropane were obtained from Sigma-Aldrich (St Louis, MO, USA). Specific primary antibodies Nrf-2 were purchased from Santa Cruz Biotechnology, Inc. (Heidelberg, Germany) and all other chemicals used were of high purity and available from commercial suppliers. The endothelial murine cells (*Mus musculus*) of axillary lymph nodes (SVEC 4-10 CRL-2181) were purchased from ATCC (American Type Culture Collection).

Preparation of CS-HA/TPP nanohydrogels

Stock solutions of CS were prepared by dissolution of the CS powder (2.5 mg ml^{-1}) in a 10% (m/v) citric acid aqueous solution or a 10% (v/v) acetic acid aqueous solution and stirred overnight. Insoluble residues were removed by centrifugation at 3800 rpm for 4 min at room temperature.

Nanohydrogels were obtained by an ionotropic gelation process [15]. An ultrasonic probe (Sonics Materials™ VC 750 Ultrasonic Processor, diameter 13 mm, ultrasonic power 750 W, frequency 20 kHz) was immersed in the CS solution (9 ml). The sonication (amplitude 32%, for 1 min 45 s) was started simultaneously with the dropwise addition of the polyanionic phase, i.e. HA (0.8 ml^{-1}) and TPP (concentrations ranging from 0.6 to 2.4 mg ml^{-1} in water (4.5 ml) and stopped at the end of the addition. Magnetic stirring was then maintained for 10 min. Unloaded nanohydrogels were obtained in the same way, omitting GdDOTA in the preparation. For cytotoxicity studies, NGs were purified by dialysis to adjust pH close to neutrality (3 × 12 h against sterile water for injection, membrane cut-off 25 kDa).

Particle size analysis by DLS

Averaged hydrodynamic diameters (Z-ave) of nanohydrogels were determined by DLS with a Zetasizer Nano ZS (Malvern Zetasizer Nano-ZS, Malvern Instruments, Worcestershire, UK). Z-average sizes are the most reliable data given by the Zetasizer Nano-ZS as they are directly determined by cumulant analysis of the correlation function. Z-average sizes are intensity averages. For each nanosuspension polydispersity indexes (PdIs) were determined by cumulant analysis. Each nanosuspension was analyzed in triplicate at 20 °C at a scattering angle of 173°, after 1/20 dilution in water. Water for injection was used as a reference dispersing medium. ζ-(zeta) potential data were collected through electrophoretic light scattering at 20 °C, 150 V, in triplicate for each sample, after 1/20 dilution in water. The instrument was calibrated with a Malvern—68 mV standard before each analysis cycle.

Asymetrical flow field flow fractionation—AF4 analysis

GdDOTA ⊂ CS-TPP/HA nanosuspensions were analyzed by an Eclipse 3 asymmetrical flow field-flow fractionation (AF4) system (Wyatt Technology, France). The dimensions of the channel were 320 × 100 × 145 mm. The accumulation wall consists of an ultrafiltration membrane (polyether sulfone (PES)—cut-off 10 kDa—Superon, Germany). A trapezoidal poly(tetrafluoroethylene) (PTFE) spacer (so called asymmetrical) delimits the area where the fractionation takes place. For the analyses, a 350 μm spacer has been selected. All injections were performed with a Shimadzu CBM-20A HPLC loop of 20 μl. For that, GdDOTA ⊂ CS-TPP/HA NGs were dispersed in water for injection at pH 7. Flow rates were controlled using a Shimadzu LC-20AB isocratic pump equipped with a micro-vacuum degasser. The eluant was passed through a vacuum degasser into the Eclipse Flow Box (Wyatt Inc. USA), before entering the AF4 channel (Wyatt Inc. USA). The laminar outflow rate was adjusted nominally to 1 ml min^{-1} while the cross flow rate was 2 ml min^{-1} for 10 min, decreased linearly to 0.1 ml min^{-1} during 15 min, and finally maintained at 0.1 ml min^{-1} during 7 min. After

fractionation, the effluent was directed to the detection chain consisting in a variable-wavelength UV–vis spectrophotometer (SPD-M20A, Shimadzu France) tuned to 254 nm, with a multi-angle light scattering (MALS) detector (ConSenxus, Ober-Hilbersheim, Germany). Data from the MALS detector were collected and processed using the Chromatographica software (ConSenxus, Ober-Hilbersheim, Germany). Calibration of the retention time should be conducted using a known internal reference material comprising the same core material as the target analyte (or as closely matched as possible). AF4 calibration based upon the equivalent sphere radius (Rs) evaluation was performed according to a recently proposed strategy that consisted of using polystyrene standard reference materials (PS) [27]. The advantages of this approach are the convenient light-scattering characterization that can be achieved for PS analytes and the well-known hydrodynamic behavior of this spherical shape for nanohydrogels particles. Delay volume and nanoparticle size normalization were determined using certified polystyrene standard latex samples with selected sizes of 23 ± 2 nm, 46 ± 2 nm, 70 ± 3 nm, 100 ± 3 nm (Duke-Thermo Scientific USA). By using static light scattering coupled on-line to the AF4, the radius of gyration, Rg, can be determined. The Rg parameter was recently shown to be more accurate for the determination of the size for asymmetrical shapes because it takes into account the mass distribution due to the shape variation that can occur during the elution process through the AF4 channel [28]. Moreover, without considering the shape of the characterized object, Rg can be directly assimilated to the hydrodynamic radius by using the shape factor ($\rho = \mathrm{Rg}/\mathrm{R_H}$) [29], using a published calculation method [27].

AFM—peak force quantitative nanomechanical mapping (AFM-PFQNM)

CS-TPP/HA and GdDOTA ⊂ CS-TPP/HA nanosuspensions were analyzed by AFM in solution in order to afford minimum perturbation of the samples [30, 31]. 35 μl of each nanosuspension was directly spread on freshly cleaved mica disks. After 20 min of deposition at ambient temperature, the sample was rinsed several times in distilled water. Nanosuspensions were then imaged in distilled water, under manually operated-PeakForce Tapping (PFT) mode on a Multimode AFM equipped with a Nanoscope V controller (Bruker, Billerica, USA). The average PeakForce setpoint was set around 100 pN, which was found to be a good compromise to remain in good tracking conditions and to avoid particle damaging. ScanAsyst Air probes (Bruker, Billerica, USA) with an average nominal spring constant of $0.4\ \mathrm{N\,m^{-1}}$ were used. For each sample, a minimum of 3 distant spots were investigated. For image processing, all images were analyzed and particle diameters were estimated using Nanoscope Analysis (Bruker, Billerica, USA). For the particle analysis, only individual and well-distinguished nanoparticles were taken into consideration and to get reliable statistical results, the analyses were performed at least on 3 different samples for each condition with around 3 images for each sample. With respect to the Young's modulus determination, force curves were automatically captured on the liquid nanosuspensions, and the linear portion of the indentation part of the extension curves were fitted using a Sneddon fit to extract the modulus. In order to display quantitative results, the tip was calibrated as detailed in the manual provided by the manufacturer. Briefly, a force curve was captured on a non-compliant sample to determine the deflection sensitivity which was always found to be between 20 and $30\ \mathrm{nm\,V^{-1}}$. Afterwards the tip was retracted 100 μm at least from the surface to avoid any influence from the support, and the spring constant was calculated via the thermal tune feature (and found to be between 0.12 and $0.63\ \mathrm{N\,m^{-1}}$. The real tip radius was calculated by imaging a tip-check sample also provided by the manufacturer, after imaging the nanoparticles. This tip estimate was used to extract the Young's modulus from the PeakForce Capture image.

Determination of nanohydrogel gadolinium content

Gadolinium nanoparticle loading was determined on raw, purified and concentrated nanosuspensions by ICP-OES. The non-encapsulated complexes were separated from the NGs by high speed centrifugation for 1 h 15 min at 4 °C and 23 200 g (Beckman Avanti™ J-E Centrifuge, France). The NP pellet was then incubated overnight in a 1:3 (v:v) mixture of HCl (37%) and HNO_3 (69%) in order to release Gd from the polymer matrix and the complexes [15, 16]. After the NG destruction, volumetric dilutions were carried out to achieve an appropriate Gd concentration within the working range of the method. Samples were analyzed using Thermo Scientific iCAP 6300 series Duo ICP spectrometer. Counts of Gd were correlated to a Gd calibration curve generated by mixing $Gd(NO_3)_3$ standard with unloaded NGs incubated under the same acidic conditions.

In vitro cytotoxicity studies

Dialyzed GdDOTA ⊂ CS-TPP/HA NGs were used for all *in vitro* studies. Before cascade dilutions, Gd concentrations were 49 μM and 98 μM for nanosuspensions obtained in citric and acetic acid respectively (ICP-OES titration).

SVEC 4-10 cells were grown in Dulbecco Modified Eagle Medium (DMEM) supplemented with 10% fetal bovine serum (FBS), 1% antibiotics (penicillin, streptomycin and amphotericin B) and maintained at 37 °C in a humidified atmosphere (95%) with 5% CO_2. The medium was changed once every three days and daily observations were made by phase contrast microscopy. The next day, the medium was replaced by either unloaded or Gd-loaded NGs diluted in FBS-supplemented DMEN. The ratio $\frac{\mathrm{volume_{nanosuspension}}}{\mathrm{volume_{FBS-supDMEN}}}$ was equal to 0.2 to maintain constant the medium osmolarity [15, 16]. Cells were incubated for 6 and 24 h with various Gd concentrations (between 1 and 10 μM for cytotoxicity tests −2.5 and 10 μM for oxidative stress studies).

Sulforhodamine B (SRB) assay. Cell viability in the presence of GdDOTA ⊂ CS-TPP/HA NGs was tested

using the commercial kit (*In Vitro* Toxicology Assay Kit, Sulforhodamine B based-Sigma-Aldrich *USA*) according to manufacturer's instructions. SVEC 4-10 cells were fixed for 1 h at 4 °C with 50% trichloroacetic acid (TCA) solution (1/4 volume of growth medium). Then, cells were washed with distilled water a few times and stained with 0.4% sulforhodamine B (Acid Red 52) for 20 min at room temperature. Afterwards the dye was removed and the cells rinsed quickly with 1% acetic acid. The incorporated dye was then solubilized in a 10 mM Tris solution. The absorbance was spectrophotometrically measured at a wavelength of 550 nm using an Appliskan Thermo Scientific Multireader.

Lactate dehydrogenase (LDH) assay. LDH activity was measured in the culture media of control and treated cells using the *In Vitro* Toxicology Assay Kit, Lactic Dehydrogenase based (Sigma-Aldrich, USA), following manufacturer's instructions. The loss of intracellular LDH and its release into the culture medium is an indicator of irreversible cell death due to cell membrane damage [32]. SVEC 4-10 cells were seeded in 24-well plates at a density of 2×10^5 cells ml^{-1} incubated overnight allowing the cells to adhere. Then, they were exposed for 6 and 24 h, to doses of 1, 2.5, 5 and 10 μM of GdDOTA $\subset$ CS-TPP/HA NGs. After that, a volume of 50 μl of culture supernatant from each well was incubated with 100 μl of LDH reaction solution for 30 min at room temperature in a 96-well plate. The reaction was stopped with HCl 1 M and the absorbance was measured at 450 nm using a microplate reader (Tecan GENios). The results were expressed relative to control (cells treated with CS-TPP/HA NPs).

Preparation of cell lysate. After exposure to nanohydrogels, SVEC4-10 cells harvested from culture flasks, were washed with phosphate buffered saline (PBS), trypsinized using 0.25% trypsin and 0.53 mM ethylenediaminetetraacetic acid (EDTA) and then centrifuged at 1500 rpm for 5 min at 18 °C. Cell pellets were resuspended in 0.3 ml of PBS and then sonicated three times with UP50H ultrasonic processor on ice, for 30 s each. The cellular lysate was centrifuged at 3000 rpm for 10 min at 4 °C. The supernatants were used for the determination of protein concentration by Bradford method, malondialdehyde (MDA), reduced glutathione (GSH) levels and Western Blot analysis.

Protein concentration assay. Total protein content was determined according to Bradford method [33] using bovine serum albumin as standard. The absorbance was measured at 595 nm using the Appliskan Thermo Scientific multireader.

Reduced glutathione (GSH) assay. Glutathione concentration was quantified using the Glutathione Assay Kit from Sigma-Aldrich, following manufacturer's instructions, in the presence of 1.5 mg ml^{-1} 5, 5-dithio-bis-2-nitrobenzoic acid. In order to determine the amount of GSH in the cellular lysates deproteinized with a 5% sulfosalicylic acid solution, a standard curve of GSH in the range of 0.5–0.03 nmoles was used. The reaction was monitored at 412 nm and the results were expressed in nmoles GSH/mg of protein.

Malondialdehyde (MDA) assay. The level of malondialdehyde was assessed by a fluorimetric method described by Dinischiotu *et al* [34]. To 200 μl cell lysate with a protein concentration of 3 mg ml^{-1}, 700 μl of 0.1 M HCl were added. The mixture was incubated for 20 min at room temperature. Then, 900 μl of 0.025 M thiobarbituric acid (TBA) were added and the mixture was incubated for 65 min at 37 °C. Finally, a volume of 400 μl of PBS buffer was added. The fluorescence of MDA was measured at 520/549 nm (excitation/emission) using a spectrofluorometer FP-750. The data were calculated as nmoles of MDA/mg of protein using a calibration curve with 1, 1, 3, 3-tetramethoxypropane in the range 0.5–5 μM.

Western blotting. The expression of protein Nrf-2 was evaluated by a Western Blot analysis using CS-TPP/HA NPs as controls. Quantities of 25 μg protein were separated by sodium dodecylsulfate polyacrylamide gel (SDS-PAGE) electrophoresis (10% polyacrylamide gels) at 70–90 V and transferred at 350 mA for 1.5 h onto 0.4 μm polyvinylidene difluoride (PVDF) membrane (Millipore, USA) in a wet transfer system (BioRad, USA). The membranes were treated with blocking solutions included in the Western Breeze Chromogenic kit (Invitrogen, USA) for 30 min at room temperature. After the incubation with primary antibodies (Nrf-2 1:250, Santa Cruz Biotechnology, USA) the membranes were processed following the kit instructions, using anti-rabbit secondary antibodies coupled with alkaline phosphatase and BCIP/NBT as the chromogenic substrate. β-Actin was used as a reference protein. Protein bands were visualized with the Bio-Rad ChemiDoc Imaging System (Bio-Rad, Hercules, CA, USA) and protein expression was quantified with the Bio-Rad Image Lab software (version 5.2, Bio-Rad, Hercules, CA, USA). Densitometry quantification of bands for Nrf-2 protein expression was normalized to β-actin and expressed relative to unloaded CS-TPP/HA NGs.

Statistical analysis. All the results were analyzed using Student's t test (Microsoft Excel) and expressed as a mean value with its standard deviation indicated (mean $\pm$ SD). A p value < 0.05 was considered statistically significant. Data were represented as graphics relative to control which was considered 100%. Each test was performed in three independent experiments.

Relaxivity measurements

^{1}H NMRD profile of GdDOTA $\subset$ CS-TPP/HA NGs concentrated by ultrafiltration (Vivaspin 100 kDa Sartorius, 4500 rpm twice ten minutes) was measured on a Stelar Spinmaster FFC fast field cycling NMR relaxometer (Stelar, Mede, Pavia, Italy) over a range of magnetic fields extending from 0.24 mT to 0.7 T and corresponding to ^{1}H Larmor

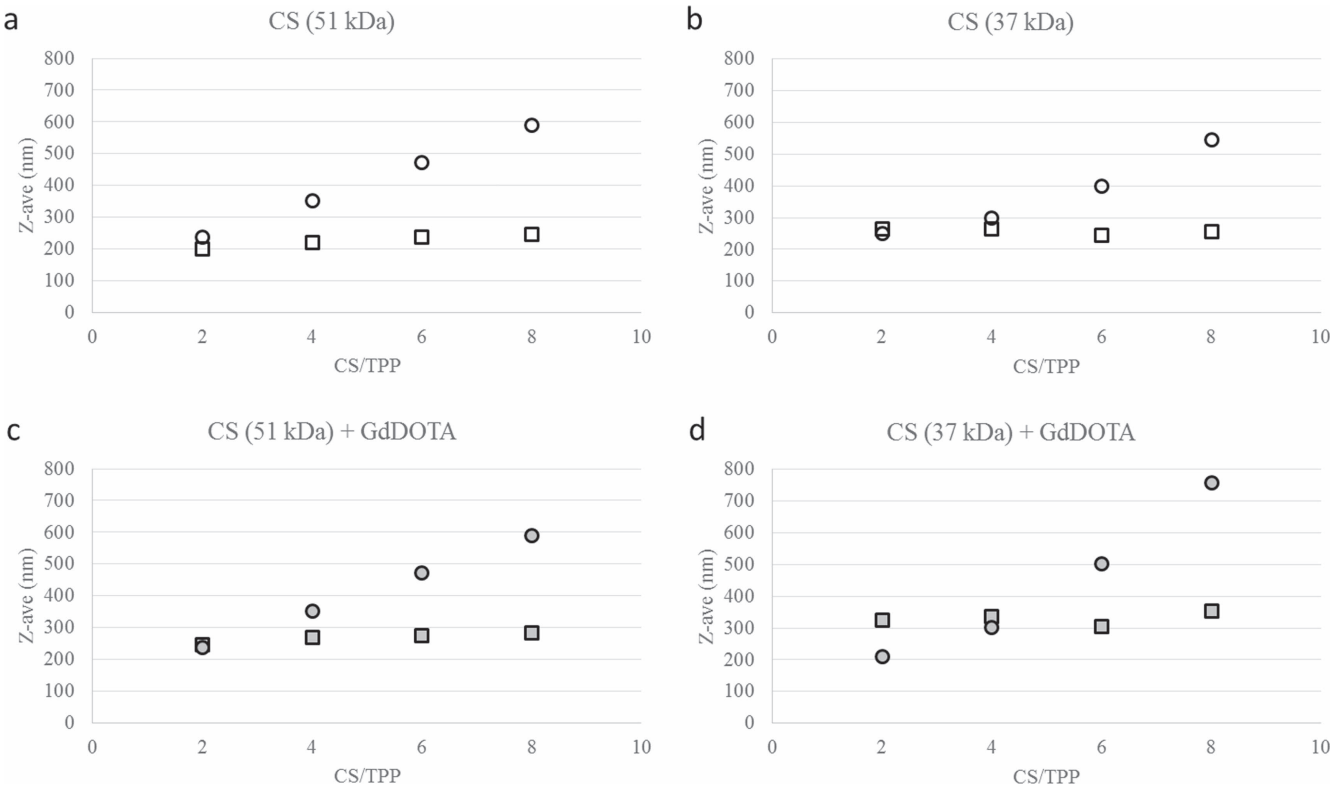

Figure 1. Intensity weighted (Z-average) diameters of CS-TPP/HA nanohydrogels obtained with (a) CS51and (b) CS37 and GdDOTA ⊂ CS-TPP/HA nanohydrogels with (c) CS51 and (d) CS37 in citric acid (squares) and acetic acid (circles) ($2 < CS/TPP < 8$).

frequencies from 0.01 to 30 MHz using 0.6 ml samples in 10 mm o.d. tubes. The temperature was kept constant at 37 °C. Additional relaxation rates at 60 were obtained with Bruker Minispec mq60 spectrometer (Bruker, Karlsruhe, Germany).

Results and discussion

DLS characterization of CS-TPP/HA and GdDOTA ⊂ CS-TPP/HA nanohydrogels

In order to tune NP size, CS of 51 kDa (CS51) and 37 kDa (CS37) molecular weights were used. CS-TPP/HA and GdDOTA ⊂ CS-TPP/HA nanohydrogels were prepared by the rapid one-step ionotropic gelation process which led to homogeneous nanosuspensions [15, 16]. To determine the NG size distribution profile, dynamic light scattering (DLS) was used. DLS provides a measure of time-related light scattering fluctuations (correlation function) that depended on the particle size. This correlation function is first converted to an intensity weighted diffusion coefficient and then to an intensity weighted hydrodynamic diameter, namely Z-average value for the dispersed particles [35, 36].

Several experimental conditions were tested to produce CS-TPP/HA and GdDOTA ⊂ CS-TPP/HA nanohydrogels. Variations in the protocol were introduced such as the nature of the acid used for CS solubilization (citric/acetic acid) and CS/TPP ratio (from 0.5 to 12). In all formulations, HA concentration is maintained constant, in order to disregard the influence of this parameter on the nanoparticle size variation. Whatever CS and acid, three typical behaviors were obtained for unloaded and GdDOTA loaded nanohydrogels. For high CS/TPP ratio range (from 8 to 12), nanoparticle concentration was too low to give a valuable signal in DLS. For low CS/TPP ratio range (from 0.5 to 2), visible aggregates were formed which rapidly sedimented. For CS/TPP ratio range between 2 and 8, stable and homogeneous nanosuspensions were obtained. All nanosuspensions exhibited positive ζ potentials (around 50 mV) which varied only slightly with CS/TPP ratio. In citric acid, an intensity-averaged diameter of 250 nm was observed for nanohydrogels synthesized with CS51 and CS37 (figure 1).

In acetic acid, NP diameters were superior (between 240 and 750 nm) for both CS51 and CS37. Then, DLS measurements showed that a decrease in CS molecular weight did not lead to smaller NGs. Nevertheless, one should note that in acetic acid, the higher the CS/TPP ratio, the larger the NG size. This result, already observed by Giacalone *et al* [26] was directly correlated to the decrease in cross-linking degree, associated to the lower amount of TPP in the mixture. Therefore, less densely packed particles were obtained leading to a shift in Z-average diameters to higher values. This effect is screened when citric acid is used, probably due to the intrinsic cross-linking ability of citrate ions [37].

Besides Z-averaged diameters, the exploitation of the correlation function allowed to have an insight of the samples polydispersity (PdI) (figure 2).

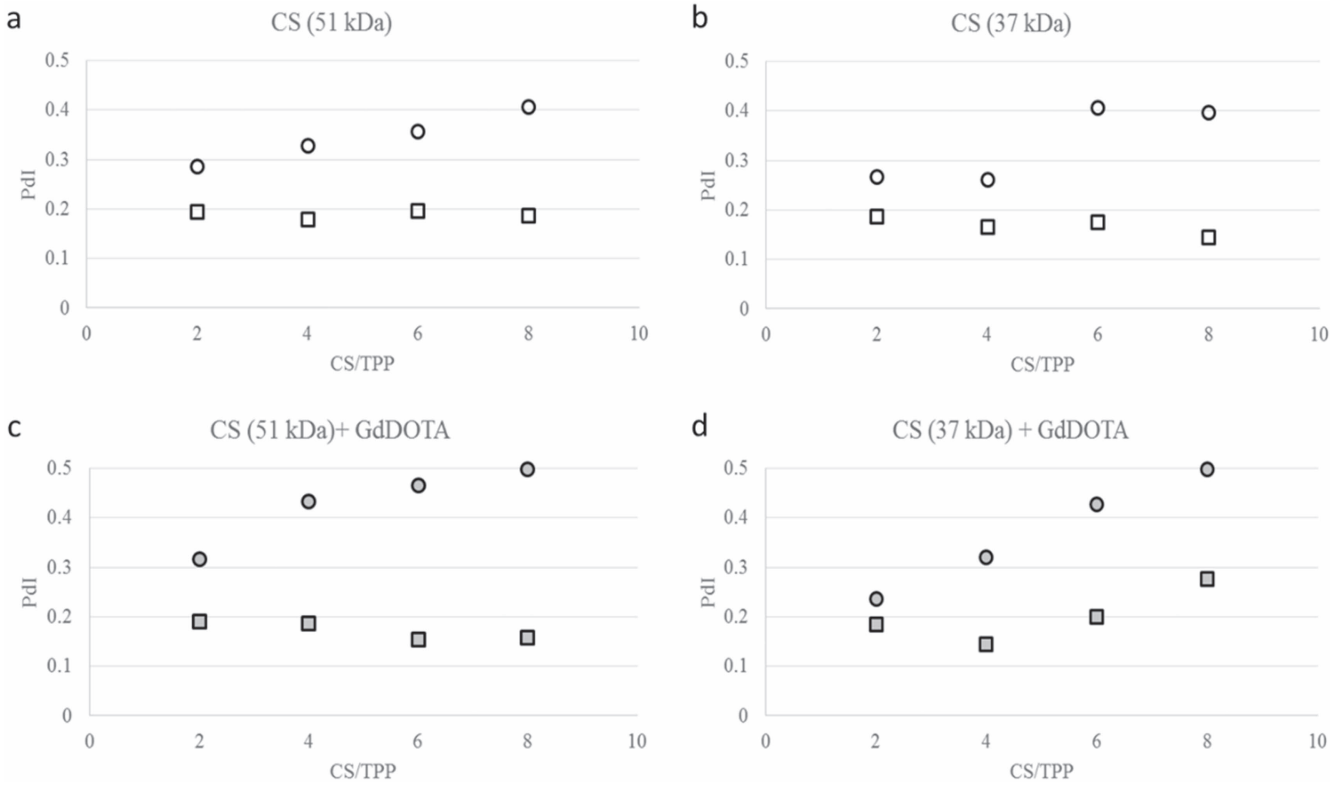

Figure 2. Polydispersity indexes (PdI) for CS-TPP/HA nanohydrogels obtained with (a) CS51 and (b) CS37 and GdDOTA ⊂ CS-TPP/HA nanohydrogels with (c) CS51 and (d) CS37 in citric acid (squares) and acetic acid (circles) ($2 < CS/TPP < 8$).

For nanosuspensions obtained in citric acid, whatever CS and CS/TPP ratio, PdI values are similar and inferior to 0.2, which indicated that nanoparticles were obtained in a narrow size range. However, in acetic acid and whatever CS, as CS/TPP ratio increased, nanosuspension polydispersity increased (PdIs > 0.3).

The presence of aggregates raise the question of the quality and the reliability of DLS analyses. This question is of an uppermost importance especially for Gd loaded nanohydrogels which could be administered. Indeed, intensity of the overall scattered light is directly proportional to the particle mass. Since the mass increases in proportion to r^3 (where r represents nanoparticle radius) larger particles, even in small amount, dominate over smaller [35, 36]. In order to get a better insight of the nanoparticle size distribution, fractionation of the nanosuspensions was undertaken by asymmetrical flow-field-flow fractionation (AF4) and NP size distribution monitored by MALS.

AF4-MALS of GdDOTA ⊂ CS-TPP/HA nanohydrogels

The general principles of the field-flow fractionation methods were first described in the late 1960s [38]. Briefly, NP separation takes place in a thin ribbon like channel in which a laminar carrier flow with a laminar flow velocity distribution is exposed to a perpendicular cross flow field. In AF4, no stationary phase is required for particle fractioning. Upon the field effect, the colloids are driven to the bottom of the channel, while diffusion causes them to be distributed at characteristic heights above the channel wall. Due to their higher diffusion coefficient, smaller particles diffuse back into the channel faster than larger particles. They leave the channel earlier, resulting in fractionation of the sample therefore providing a continuous size distribution.

All GdDOTA ⊂ CS-TPP/HA formulations were analyzed by asymetrical flow field-flow fractionation (AF4). Whatever the formulation, the corresponding elugrams exhibited a first retention peak close to the void peak ($t_R = 9.5$ min $= t_0$), that can be associated to some residual species (for instance residual CS or HA that were not engaged in the nanoparticle network). A second set of retention peaks were observed for $t_R > 9.8$ min corresponding to the nanoparticle elution. It is generally assumed that the integration of the AF4 UV signal gives an estimation of the NG percentage that corresponds to each retention peak [28]. Thus, for CS/TPP ratios of 2 and 4, the integration of the UV signal indicated that the relative quantity of residual species was less than 3% wt. For higher CS/TPP ratios this proportion strongly increased, illustrating the fact that TPP concentration was not sufficient to ensure a good NG packing. For the second set of retention peaks (and for $2 < CS/TPP < 4$) that corresponded to the nanohydrogel signal ($t_R > 9.8$ min), a recovery higher than 85% ± 5%, was obtained. This high value, which was significant, indicated that almost all the nanoparticles injected in the AF4 channel were recovered after fractionation. It also indicated that size analysis that stemmed from AF4 elugrams for formulations with CS/TPP ratios of 2 and 4 will give good indications on the nanohydrogel mean diameter distribution.

Table 1. AF4-MALS (d_{AF4} (nm)) and UV (%) analyses of GdDOTA ⊂ CS-TPP/HA nanohydrogels.

Acid	CS	CS/TPP	d_{AF4}(nm)-%population for $t_R > t_0$		
Citric	CS51	2	40 nm—16%	200 nm—62%	>500 nm—22%
	CS37		40 nm—13%		>500 nm—87%
Citric	CS51	4	40 nm—17%	300 nm—26%	>500 nm—57%
	CS37		40 nm—18%		>500 nm—82%
Acetic	CS51	2	55 nm—89%		>500 nm—11%
	CS37		75 nm—66%		>500 nm—34%
Acetic	CS51	4	60 nm—87%		>500 nm—13%
	CS37		70 nm—77%		>500 nm—23%

For Gd-loaded nanohydrogels, NP sizes distribution determined by AF4-MALS analysis showed two main populations (table 1). A first one, below 100 nm, could be ascribed to individual objects. The second one above 200 nm, divided in citric acid in two components (between 200 and 300 nm and superior to 500 nm) and in acetic acid in one component (above 500 nm), could be ascribed to aggregates.

These features were independent of CS molecular weight, corroborating the fact that lowering CS molecular weight did not induce NG mean size modification. Furthermore, mean values determined by AF4-MALS analysis were as expected, systematically inferior to those determined by DLS, since by upon AF4 fractionation, discrimination between smaller and larger nano-objects was available. Regarding the first population ($d < 100$ nm), whatever CS/TPP ratio, GdDOTA ⊂ CS-TPP/HA NGs synthesized in citric acid displayed mean sizes inferior to the ones obtained in acetic acid. This difference supported the fact that citrate ions acted as cross-linkers to improve NG packing. One should also notice that in acetic acid, individual NG proportions were higher than in citric acid. Therefore AF4 analysis is in contradiction with DLS analysis, i.e. in acetic acid interparticle cross-linkages, that should led to the formation of nanoparticle clusters, were less pronounced than in citric acid. To discriminate between the results of DLS and AF4 a third method is necessary to have a better insight on nanoparticle morphology. Therefore AFM measurements were undertaken on CS-TPP/HA and GdDOTA ⊂ CS-TPP/HA nanosuspensions, in order to get a more direct evaluation of NP diameters and to evaluate the influence of Gd chelates on nanoparticle stiffness as well.

AFM characterization of CS-TPP/HA and GdDOTA ⊂ CS-TPP/HA nanohydrogels

AFM is a sub-nanometer resolution method in the family of scanning probe microscopy [39]. It utilizes a sharp tip mounted on a reflective cantilever which is scanned over the sample surface in *X* and *Y*-directions, oscillating along *Z*-direction according to the local surface changes. Laser-based detection of cantilever oscillations allows generating a height profile of the surface which in turn can give access to a 3D-image of the sample. AFM, usually operated in tapping mode has been demonstrated to be the technique of choice to image both individual nanoparticles and particle aggregates [40–42]. In this mode, since cantilever is intermittently at the contact of object surface, friction and shear forces are negligible, making this approach ideal to image fragile samples. Most of the time, tapping mode has been used on stiff nanoparticles [43, 44] more hardly on softer samples like polyacrylic copolymers based colloids [45], polymersomes [46, 47], cisplatin-nanoencapsulated liposomes [48], or insulin/chitosan self-assembled particles [30]. Usually, AFM studies are conducted in air. In order to afford minimum perturbation of the samples, especially as nanohydrogels are concerned, and to be in conditions close to the ones used in DLS or AF4 it is preferable to analyze samples in liquids. So far, only few studies regarding AFM measurements in liquid environment have been reported [30, 31]. CS-TPP/HA and GdDOTA ⊂ CS-TPP/HA NGs morphologies were then analyzed in liquid phase with the PFT mode [49], according to CS/TPP ratios. Nanohydrogels obtained with $2 < CS/TPP < 8$ ratios were all imaged but for the sake of clarity, only NGs corresponding to CS/TPP ratios of 2 and 4 are shown.

For unloaded nanosuspensions (figure 3), under similar formulation conditions (i.e. same acid and same CS/TPP ratio) no topological differences could be noticed according to CS molecular weight. In any case, NP diameters calculated from the AFM images were highly inferior to 100 nm (table 2).

As previously suspected, CS molecular weight did not seem to have an impact on the particle diameters. This could be explained by the fact that all nanoparticles were obtained under sonication. Indeed, it has been demonstrated that ultrasonication can induce a partial depolymerization of CS, leading to NGs of smaller sizes [50]. One should then hypothesize that ultrasound effects led to a standardization of NG sizes, which sizes were therefore no more correlated with CS molecular weight. AFM height images also showed that particle density on the substrate was much more important for the lower CS/TPP ratio of 2. Indeed, under high TPP concentration, ionic interactions between CS and TPP were strengthened, leading to higher NG production yields. This feature was more pronounced in acetic acid, thereby corroborating AF4 measurements. It therefore seemed to prove that in acetic medium since no additional cross-linkers other than

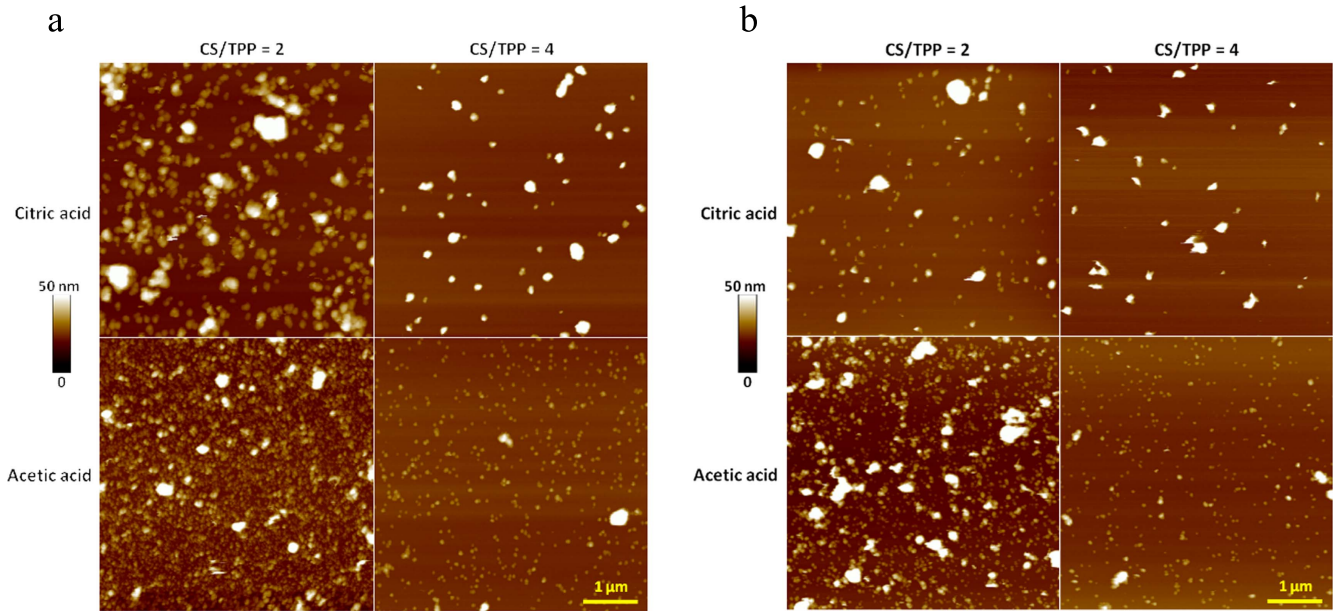

Figure 3. AFM images in PFT mode of CS-TPP/HA nanohydrogels obtained with (a) CS51and (b) CS37 for CS/TPP ratios of 2 and 4 (5 × 5 μm × 50 nm AFM height images).

Table 2. CS-TPP/HA nanoparticle diameters (d_{AFM}) in function of CS molecular weight and CS/TPP ratio.

$d_{AFM} \pm$ sd (nm)	CS51				CS37			
CS/TPP	2	4	6	8	2	4	6	8
Citric acid	44 ± 9	57 ± 9	58 ± 10	60 ± 10	77 ± 13	65 ± 16	45.0 ± 16	70 ± 10
Acetic acid	51 ± 6	46 ± 5	33 ± 10	44 ± 4	31 ± 10	28 ± 11	29.0 ± 11.6	29 ± 9

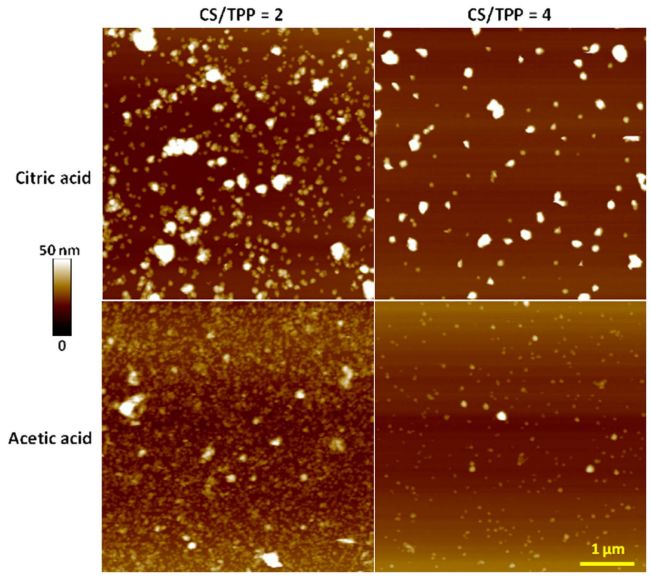

Figure 4. AFM images in PFT mode of GdDOTA ⊂ CS51-TPP/HA nanohydrogels for CS/TPP ratios of 2 and 4 (5 × 5 μm × 50 nm AFM height images).

Table 3. GdDOTA ⊂ CS51-TPP/HA nanohydrogel diameters (d_{AFM}) in function of CS/TPP ratio.

$d_{AFM} \pm$ sd (nm)	CS51			
CS/TPP	2	4	6	8
Citric acid	37 ± 10	40 ± 10	48 ± 16	47 ± 12
Acetic acid	44 ± 10	43 ± 9	38 ± 9	42 ± 9

TPP are available to reinforce the network between CS and HA, intra-cross linkages were privileged. On the contrary, in citric acid, citrate ions helped to reinforce the network between CS and HA thereby leading to more packed NGs but also acted as cross-linkers between the nanoparticles. Since ionic gelation complexation process is under kinetic control [51], under an excess of citrate ions the complexation rate could be accelerated, leaving the possibility to competitive mechanisms such as interlinks between nanoparticles to take place.

As CS molecular weight had no impact on NP sizes, only GdDOTA ⊂ CS51-TPP/HA nanohydrogels were characterized by AFM with PFT mode (figure 4). As described for unloaded NGs, sizes of GdDOTA loaded NGs were not affected by CS/TPP ratio variation (table 3) and topological characteristics of GdDOTA ⊂ CS51-TPP/HA NGs are identical to the ones of CS-TPP/HA NGs.

AFM PFT mode not only allowed to work on liquid nano-suspensions but also allowed to extract the reduced Young's modulus of nano-objects after tip calibration (see Methods section for details [49]). For unloaded NPs, the Young's modulus was found to be in the order of 2 MPa,

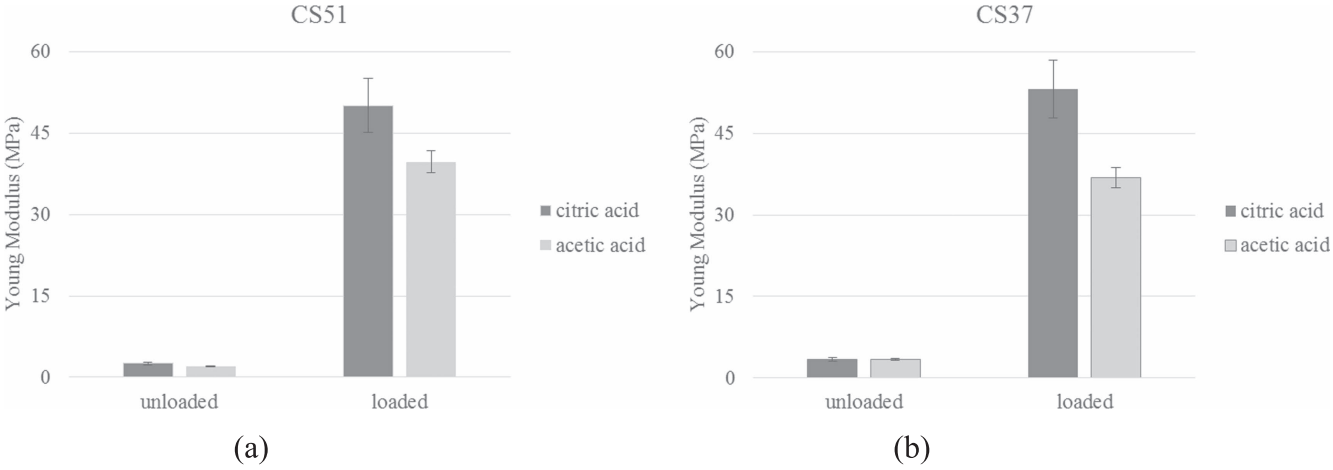

Figure 5. Evolution of the Young modulus of the (a) unloaded and (b) GdDOTA loaded CS-TPP/HA NGs in function of the acid nature.

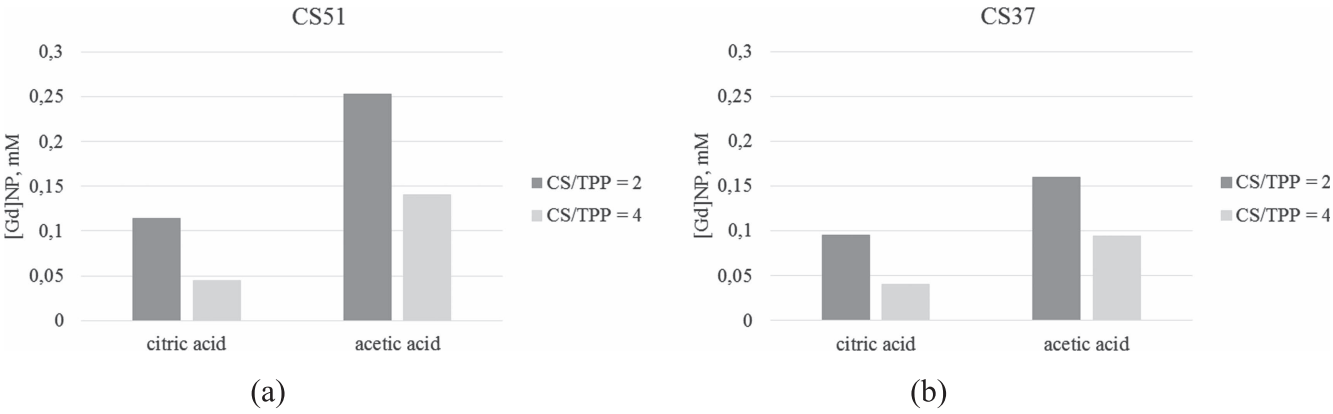

Figure 6. Gd pellet loadings of GdDOTA ⊂ CS-TPP/HA nanohydrogels in function of CS and CS/TPP ratio.

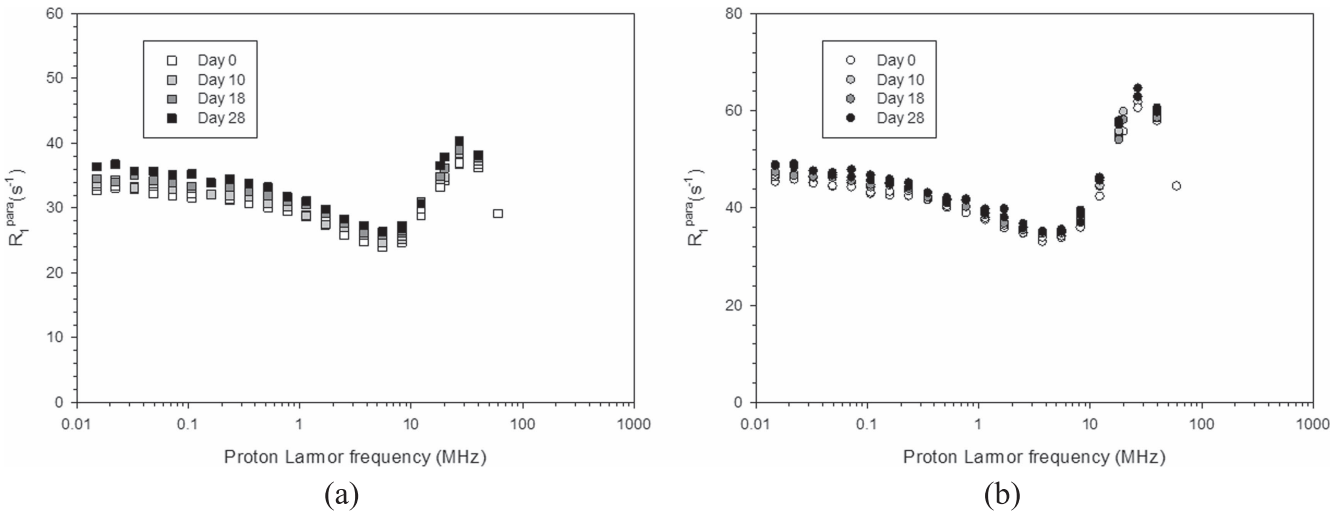

Figure 7. Time evolution of ^{1}H NMRD profiles of GdDOTA ⊂ CS51-TPP/HA NGs synthesized in (a) citric acid and in (b) acetic acid (CS/TPP = 2).

whatever CS molecular weight (2.57 and 1.98 MPa for CS51 NGs obtained in citric and acetic acid respectively and 3.37 and 3.49 MPa for CS37 NGs obtained in citric and acetic acid respectively). For GdDOTA ⊂ CS51-TPP/HA NGs, this value was typically increased by factor 20 or higher (50.11 and 39.75 MPa in average for GdDOTA loaded NGs obtained in citric and acetic acid respectively), similar value being measured for GdDOTA ⊂ CS37-TPP/HA NGs (figure 5).

Even if AFM substrate could influence NG mechanical properties, these data qualitatively indicate that the presence

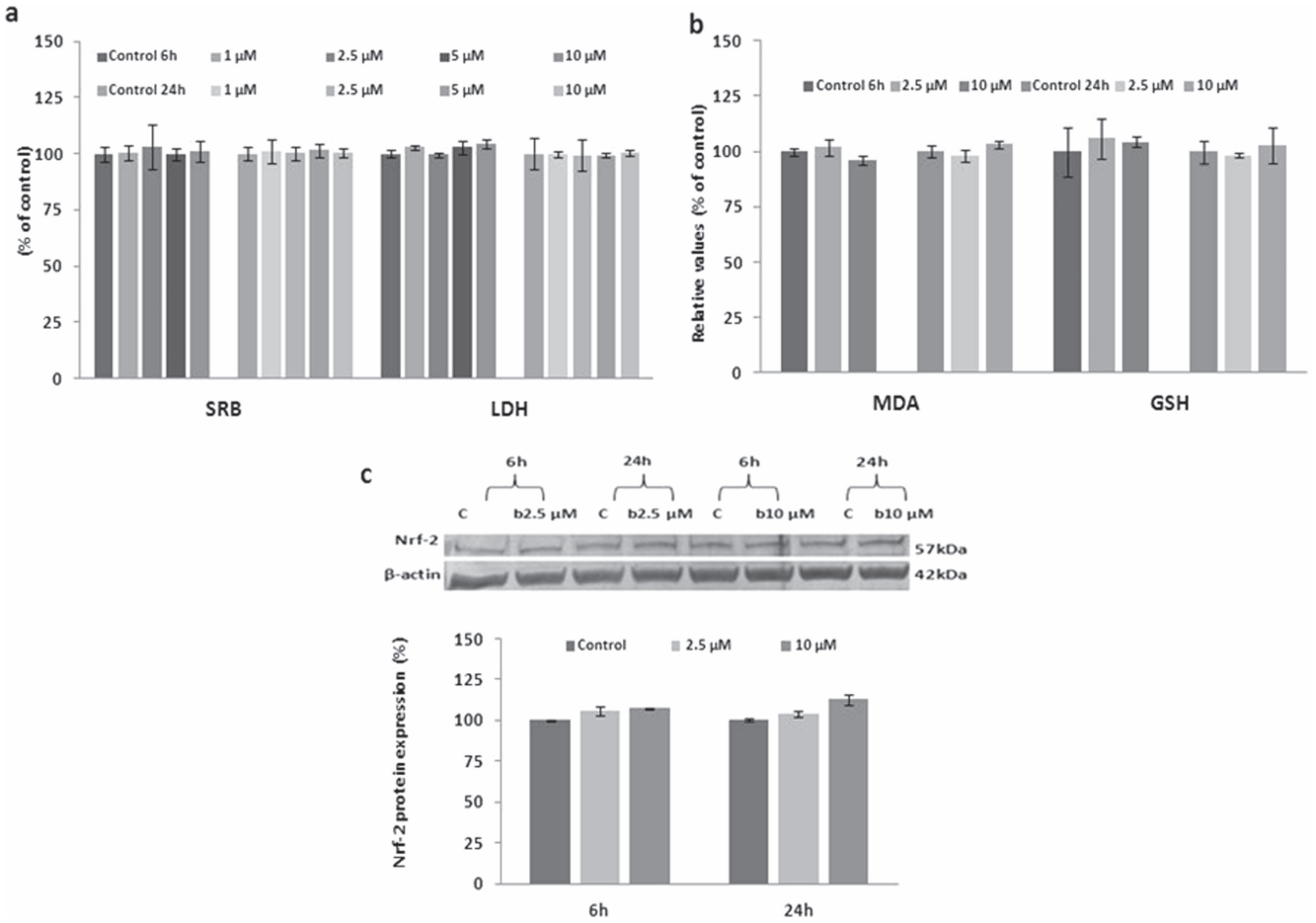

Figure 8. (a) Viability (SRB assay) and cytotoxicity (LDH release in culture medium) evaluation, (b) MDA and GSH relative concentrations, (c) Nrf-2 protein expression in SVEC4-10 cells in the presence of increased concentrations of GdDOTA ⊂ CS51-TPP/HA NGs obtained in citric acid, at 6 and 24 h exposure times. Unloaded CS51-TPP/HA NGs obtained in citric acid were used as controls. Data are expressed as average ±SD ($n = 3$).

of Gd chelates within the NPs reinforces the nanohydrogel network and increases its stiffness. This interesting result must be compared to the one obtained for enhancement of elastic modulus of ionic chitosan cryogel loaded with metal complexes [52].

GdCA loadings and MRI efficiency of relevant GdDOTA ⊂ CS-TPP/HA nanohydrogels

Gd contents of GdDOTA ⊂ CS-TPP/HA nanohydrogels obtained with CS/TPP ratios of 2 and 4, were determined by ICP-OES titrations after ultracentrifugation and NG pellet recovery (figure 6).

Whatever CS molecular weight, the amount of GdDOTA encapsulated inside nanohydrogels increased as CS/TPP decreased, i.e. as nanohydrogels were more cross-linked. This result is in good agreement with Giacalone *et al* data [26] which demonstrated that a high amount of TPP strengthened the gel network and then the electrostatic interactions between the anionic Gd chelate and the positive charges of the protonated amino functions of CS. Therefore, physical entrapment of Gd chelates was promoted. Moreover, Gd concentration was higher for nanohydrogels prepared in acetic acid. AFM images showed that in this acid, a larger number of nano-objects was produced in agreement with the AF4-MALS results showing a larger amount of small size NGs. As the NG production yield was increased in acetic acid, Gd chelate encapsulation is more important, thereby leading to an increase of the encapsulated Gd chelate quantities [53]. The data also indicated that the use of low molecular weight CS induced a decrease in Gd loading. For this reason, GdDOTA ⊂ CS37-TPP/HA were discarded from MRI evaluation. GdDOTA ⊂ CS51-TPP/HA nanohydrogels MRI efficiency was then determined by means of their longitudinal relaxation rates determination. For that NMRD profiles of GdDOTA ⊂ CS51-TPP/HA were recorded at 37 °C as a function of the nature of the acid used for CS solubilization (figure 7).

Whatever the acid, all NMRD profiles exhibited a similar shape with a maximum in the relaxation rate between 20 and 60 MHz. These enhancements indicated that inside nanohydrogels not only GdCA motions were restricted [15, 16] but also strong outer-sphere and/or second-sphere contribution to relaxation took part. This hypothesis is supported by the fact that both CS and HA are highly hydrophilic [14] and provide a favorable aqueous environment for GdCAs via H-bonding

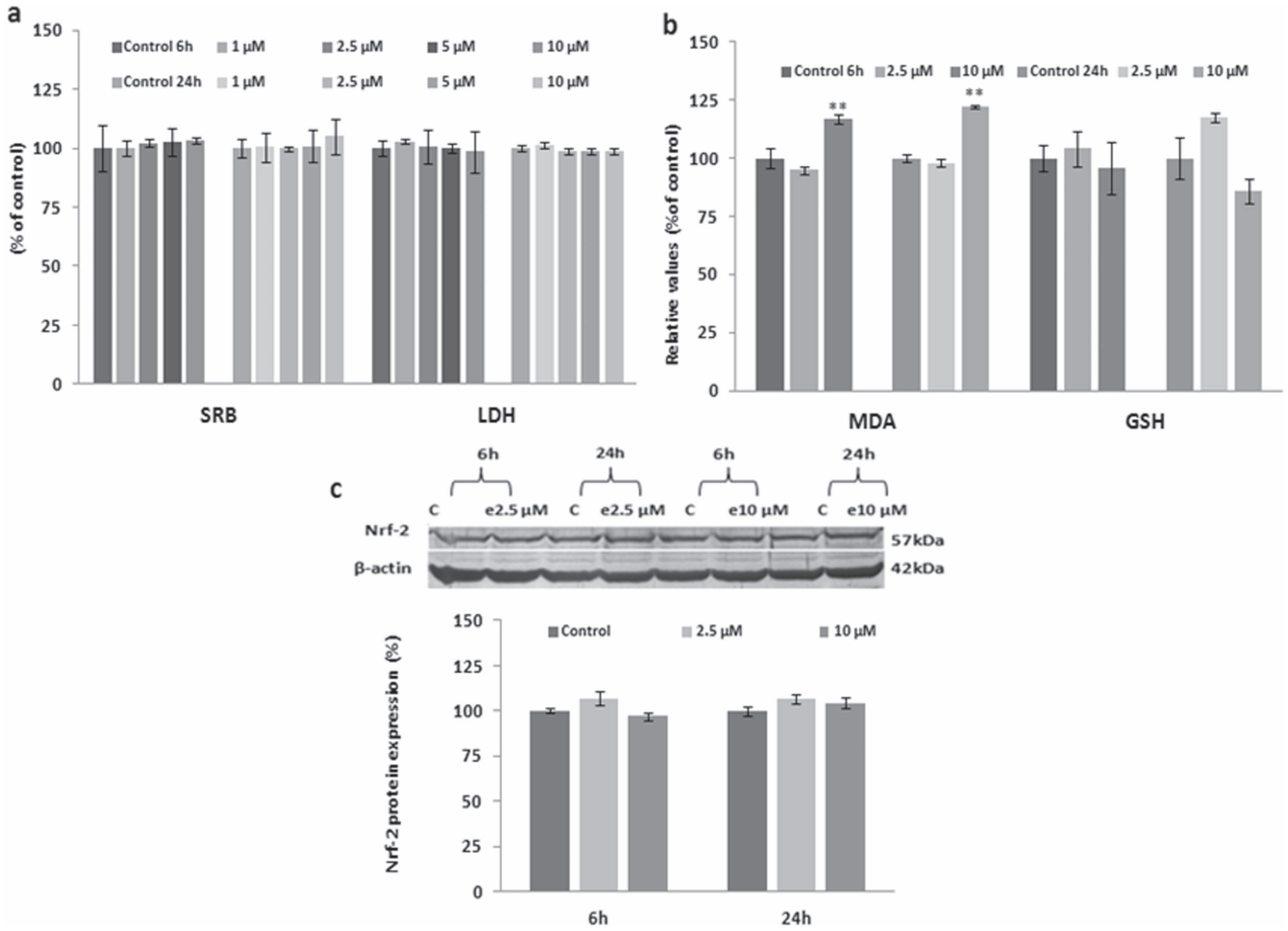

Figure 9. (a) Viability (SRB assay) and cytotoxicity (LDH release in culture medium) evaluation, (b) MDA and GSH relative concentrations, (c) Nrf-2 protein expression in SVEC4-10 cells in the presence of increased concentrations of GdDOTA ⊂ CS51-TPP/HA NGs obtained in acetic acid, at 6 and 24 h exposure times. Unloaded CS51-TPP/HA NGs obtained in acetic acid were used as controls. Data are expressed as average ± SD ($n = 3$).

interactions between water molecules and the Gd chelates. Furthermore, the profile shape is maintained over a period of 28 d which highlighted the stability of the GdDOTA ⊂ CS51-TPP/HA NGs and the lack of Gd leakage from the NP core. Therefore, this suggested that GdDOTA ⊂ CS51-TPP/HA NPs could be useful for long-term MRI detection.

Cytotoxicity studies of GdDOTA ⊂ CS51-TPP/HA nanohydrogels

Since GdDOTA ⊂ CS51-TPP/HA nanohydrogels were designed for lymph node imaging, the *in vitro* effects of Gd nanohydrogels obtained with a CS/TPP ratio of 2 (i.e. with the best Gd loadings) were evaluated on SVEC4-10 murine lymph node endothelial cell line. For this purpose Gd nanohydrogels synthesized in citric acid and in acetic acid were compared. Previous studies revealed that gadolinium-based contrast agents did not affect significantly the viability of HepG2 [54], mouse B16 melanoma [55] and A549 cells [56]. The cytotoxicity and biochemical changes induced in SVEC4-10 cells consequently to their treatment with different concentrations of GdDOTA ⊂ CS51-TPP/HA NGs were then analyzed after 6 and 24 h of exposure. The total cellular biomass and lactate dehydrogenase release in the culture medium were evaluated with SRB and LDH assays respectively, oxidative stress parameters were checked through MDA and GSH assays respectively while Nrf-2 protein expression was evaluated by Western blotting.

For endothelial SVEC4-10 cells incubated with GdDOTA ⊂ CS51-TPP/HA NGs synthesized in citric acid (figure 8), SRB test revealed no change in cell viability between the treated cells and the controls. This absence of cytotoxicity was confirmed by the LDH release results, which showed that even after 24 h and for the highest concentration tested, the cell membrane integrity was not affected.

Similar results were obtained for lipid peroxidation (MDA) and GSH levels since for SVEC4-10 cells treated with citric GdDOTA ⊂ CS51-TPP/HA NGs, these values were similar to the ones measured in the presence of relevant controls. Finally, no changes in Nrf-2 protein expression were observed as well.

For endothelial SVEC4-10 cells incubated with GdDOTA ⊂ CS51-TPP/HA NGs synthesized in acetic acid (figure 9), no major difference was observed for SRB and LDH tests compared to citric Gd nanohydrogels.

On the other hand, exposure of cells to the highest concentration of acetic GdDOTA ⊂ CS51-TPP/HA NGs induced a significant increase of MDA level, by 16% and 22% after 6 and 24 h respectively. In the meantime, a decrease of GSH concentration by 15% after 24 h was noticed. However, no significant changes were observed in Nrf-2 expression.

To sum up, these data suggested that citric Gd nanohydrogels have good biocompatibility against SVEC4-10 cells. For both citric and acetic Gd nanohydrogels, their interaction with endothelial cells might generate reactive oxygen species which can be counteracted by cellular antioxidant system. Probably, the formation of ROS did not occur because the expression of antioxidant gene Nrf-2, involved in the maintenance of redox homeostasis and cell survival [57, 58] was not changed when cells were treated with Gd nanohydrogels or controls.

Conclusion

To sum up and conclude, our objective was to improve GdDOTA ⊂ CS-TPP/HA NG sizes in order to favor their access to lymph nodes. For that, variation of formulation parameters known to influence nano-object sizes, i.e. CS molecular weight and CS/TPP ratio, was attempted. NP sizes and morphologies were systematically determined by means of DLS, AF4 and AFM in liquid mode, which allowed to conclude that from an analytical point of view, DLS data should be systematically consolidated by AF4 or by AFM in liquid mode. This last technique is particularly well suited since AFM experimental conditions are less invasive for nanogels and no application of mathematical models is required to obtain size information. From a formulation point of view, decrease of CS molecular weight as well as CS/TPP ratio did not induce nano-object size decrease, probably because the shear forces induced by ultrasonication led to a standardization of nano-object sizes, which were no more correlated to CS molecular weight or to CS/TPP ratio. On the other hand, CS/TPP ratio influenced the nanoparticle density in nanosuspensions since low CS/TPP led to a high particle density. At this level, the acid used for CS solubilization has a significant influence since in acetic acid, the amount of formed nanoparticles is higher than in citric acid. Therefore GdDOTA loading was improved for NGs obtained in acetic acid. From an MRI point of view, whatever the acid, GdDOTA ⊂ CS-TPP/HA NGs exhibited a good ability to increase R_1 longitudinal relaxation rates and then MRI efficiency at 1.5 T. Another interesting feature for MRI application is the NMRD signal persistence over one month. This highlighted the lack of Gd leakage from nanogels that has to be correlated with gel stiffness improvement evaluated by AFM-QNM for GdDOTA ⊂ CS-TPP/HA NGs, by comparison with unloaded CS-TPP/HA NGs. Finally, cytotoxicity evaluation of GdDOTA ⊂ CS-TPP/HA NGs indicated that they presented low toxicity for SVEC4-10 cells. The slight increase observed for MDA levels suggested that cell antioxidant defense mechanisms counteract efficiently the oxidative stress induced by the exposure of cells to these nanohydrogels. Therefore, GdDOTA ⊂ CS-TPP/HA NGs are good candidates for long-term MR imaging of lymph nodes, which is currently being investigated.

Acknowledgments

The work was supported by ANR (Gadolymph project n° ANR-13-ENM2-0001-01, through the EuroNanoMed 2013 framework), by the Région Wallone (Gadolymph project n° 1317980 through the EuroNanoMed 2013 framework), by the Romanian National Authority for Scientific Research CCCDI-UEFISCDI (project number 4-006/2014, EuroNanoMed II), by the Region Champagne Ardenne, the DRRT Champagne Ardenne (through MESR) and the EU-program FEDER (Project NanoBio2, Nano'Mat Platform). The ARC (research contract AUWB-2010—10/15-UMONS-5), the FNRS, ENCITE program, the COST TD1004 (Theranostics imaging and therapy: an action to develop novel nanosized systems for imaging-guided drug delivery), the UIAP VII program and the Center for Microscopy and Molecular Imaging (CMMI, supported by the European Regional Development Fund and the Walloon Region) are thanked for their support. The AF4 work has been, in part, supported by a grant from the French National Agency for Research called 'Investissements d'Avenir', Equipex Arronax-Plus no ANR-11-EQPX-0004 and Labex no ANR-11-LABX-0018-01. KiOmed Pharma (Herstal, Belgium) is gratefully acknowledged for providing the KiOmedine® ultrapure chitosan CS37 and its characterization as well as Amandine Destrebecq for her help in ICP-OES titrations.

References

[1] Caravan P 2006 Strategies for increasing the sensitivity gadolinium based MRI contrast agents *Chem. Soc. Rev.* **35** 512–23

[2] Merbach A E, Helm L and Toth E 2013 *The Chemistry of Contrast Agents in Medical Magnetic Resonance Imaging* 2nd edn (Chichester: Wiley)

[3] Terreno E, Delli Castelli D, Viale A and Aime S 2010 Challenges for molecular magnetic resonance imaging *Chem. Rev.* **110** 3019–42

[4] Hermann P, Kotek J, Kubıcek V and Lukes I 2008 Gadolinium (III) complexes as MRI contrast agents: ligand design and properties of the complexes *Dalton Trans.* **23** 3027–124

[5] Helm L 2006 Relaxivity in paramagnetic systems: theory and mechanisms *Prog. Nucl. Magn. Reson. Spectrosc.* **49** 45–64

[6] Tang J, Sheng Y, Hu H and Shen Y 2013 Macromolecular MRI contrast agents: structures, properties and applications *Prog. Polym. Sci.* **38** 462–502

[7] Delli Castelli D, Gianolio E, Geninatti Crich S, Terreno E and Silvio Aime S 2008 Metal containing nanosized systems for MR-molecular imaging applications *Coord. Chem. Rev.* **252** 2424–43

[8] Aime S, Frullano L and Geninatti Crich S 2002 Compartmentalization of a gadolinium complex in the apoferritin cavity: a route to obtain high relaxivity contrast

agents for magnetic resonance imaging *Angew. Chem., Int. Ed.* **41** 1017–9
[9] Ananta J S *et al* 2010 Geometrical confinement of gadolinium-based contrast agents in nanoporous particles enhances T_1 contrast *Nat. Nanotechnol.* **5** 815–21
[10] Karimdjy M M, Tallec G, Fries P H, Imbert D and Mazzanti M 2015 Confinement of a tris-aqua Gd(III) complex in silica nanoparticles leads to high stability and high relaxivity and supresses anion binding *Chem. Commun.* **51** 6836–8
[11] Rigaux G *et al* 2014 A new magnetic resonance imaging contrast agent loaded into poly(lactide-co-glycolide) nanoparticles for long-term detection of tumors *Nanotechnology* **25** 445103–14
[12] Malzahn K *et al* 2016 Design and control of nanoconfinement to achieve magnetic resonance contrast agents with high relaxivity *Adv. Health. Mater.* **5** 567–74
[13] Ni K, Zhao Z, Zhang Z, Zhou Z, Yang L, Wang L, Ai H and Gao J 2016 Geometrically confined ultrasmall gadolinium oxide nanoparticles boost the T_1 contrast ability *Nanoscale* **8** 3768–74
[14] Dong R, Pang Y, Su Y and Zhu X 2015 Supramolecular hydrogels: synthesis, properties and their biomedical applications *Biomater* **3** 937–54
[15] Courant T *et al* 2012 Hydrogels incorporating GdDOTA: towards highly efficient dual T_1/T_2 MRI contrast agents *Angew. Chem., Int. Ed.* **51** 9119–22
[16] Callewaert M *et al* 2014 Tuning the composition of biocompatible Gd nanohydrogels to achieve hypersensitive dual T_1/T_2 MRI contrast agents *J. Mater. Chem.* B **2** 6397–405
[17] Garcia-Fuentes M and Alonso M J 2012 Chitosan-based drug nanocarriers: Where do we stand? *J. Control. Release* **161** 496–504
[18] Kean T and Thanou M 2010 Biodegradation, biodistribution and toxicity of chitosan *Adv. Drug. Deliv. Rev.* **62** 3–11
[19] Kogan G, Soltes L, Stern R and Gemeiner P 2007 Hyaluronic acid: a natural biopolymer with a broad range of biomedical and industrial applications *Biotechnol. Lett.* **29** 17–25
[20] Lee J Y and Spicer A P 2000 Hyaluronan: a multifunctional, megaDalton, stealth molecule *Curr. Opin. Cell Biol.* **12** 581–6
[21] Misselwitz B 2006 MR contrast agents in lymph node imaging *Eur. J. Radiol.* **35** 375–82
[22] Ferreira S A, Gama F M and Vilanova M 2013 Polymeric nanogels as vaccine delivery systems *Nanomedicine* **9** 159–73
[23] Almalik A, Donno R, Cadman C J, Cellesi F, Day P J and Tirelli N 2013 Hyaluronic acid-coated chitosan nanoparticles: molecular weight-dependent effects on morphology and hyaluronic acid presentation *J. Control. Release* **172** 1142–50
[24] Calvo P, Remunan-Lopez C, Vila-Jato J L and Alonso M J 1997 Novel hydrophilic chitosan–polyethylene oxide nanoparticles as protein carriers *J. Appl. Polym. Sci.* **63** 125–32
[25] Gan Q, Wang T, Cochrane C and McCarronb P 2005 Modulation of surface charge, particle size and morphological properties of chitosan–TPP nanoparticles intended for gene delivery *Colloid Surf. B: Biointerfaces* **44** 65–73
[26] Giacalone G, Bochot A, Fattal E and Hillaireau H 2013 Drug-induced nanocarrier assembly as a strategy for the cellular delivery of nucleotides and nucleotide analogues *Biomacromolecules* **14** 737–42
[27] Gigault J and Hackley V A 2013 Observation of size-independent effects in nanoparticle retention behavior during asymmetric-flow field-flow fractionation *Anal. Bioanal. Chem.* **405** 6251–8
[28] Gigault J, Zhang W, Lespes G, Charleux B and Grassl B 2014 Asymmetrical flow field-flow fractionation analysis of water suspensions of polymer nanofibers synthesized via RAFT-mediated emulsion polymerization *Anal. Chim. Acta* **819** 116–21
[29] Burchard W 1983 Static and dynamic light scattering from branched polymers and biopolymers *Light Scattering for Polymers Springer, Advances in Polymer Science* ed W Burchard and G D Peterson vol 48 (Berlin: Springer) pp 1–124
[30] Best J P, Neubauer M P, Javed S, Dam H H, Fery A and Caruso F 2013 Mechanics of pH-responsive hydrogel capsules *Langmuir* **29** 9814–23
[31] Cui J, Björnmalm M, Liang K, Best J P, Zhang X and Caruso F 2014 Super-soft hydrogel particles with tunable elasticity in a microfluidic blood capillary model *Adv. Mater.* **29** 7295–9
[32] Fotakis G and Timbrell J A 2006 *In vitro* cytotoxicity assays: comparison of LDH, neutral red, MTT and protein assay in hepatoma cell lines following exposure to cadmium chloride *Toxicol. Lett.* **160** 171–7
[33] Bradford M M 1976 A rapid and sensitive method for the quantitation of microgram quantities of protein utilizing the principle of protein-dye binding *Anal. Biochem.* **72** 248–54
[34] Dinischiotu A, Stanca L, Gradinaru D, Petrache S N, Radu M and Serban A 2013 Lipid peroxidation due to *in vitro* and *in vivo* exposure of biological samples to nanoparticles *Oxidative Stress and Nanotechnology: Methods and Protocols, Methods in Molecular Biology* ed D Armstrong and D J Bharali vol 1028 (New York: Springer Science Business Media) ch 10 pp 155–64
[35] Lapresta-Fernandez A *et al* 2014 A general perspective of the characterization and quantification of nanoparticles: imaging, spectroscopic, and separation techniques *Crc. Cr. Rev. Sol. State* **39** 423–58
[36] Uskokovic V 2012 Dynamic light scattering based microelectrophoresis: main prospects and limitations *J. Disper. Sci Technol.* **33** 1762–86
[37] Murthy V S, Rana R K, Michael S and Wong M S 2006 Nanoparticle-assembled capsule synthesis: formation of colloidal polyamine-salt intermediates *J. Phys. Chem.* B **110** 25619–27
[38] Giddings J C 1966 A new separation concept cased on a coupling of concentration and flow non uniformities *Sept. Sci.* **1** 123–5
[39] Binnig G, Quate C F and Gerber C 1986 Atomic force microscope *Phys. Rev. Lett.* **56** 930–3
[40] Liu F K, Chang Y C, Ko F H, Chu T C and Dai B T 2003 Rapid fabrication of high quality self-assembled nanometer gold nanoparticles by spin coating method *Microelectron. Eng.* **67–68** 702–9
[41] Xia D, Biswas A, Li D and Bruek S 2004 Directed self-assembly of silica nanoparticles into nanometer-scale patterned surfaces using spin coating *Adv. Mater.* **16** 1427–32
[42] Juillerat F, Bowen H H and Hofmann H 2005 Fabrication of large-area ordered arrays of nanoparticles on patterned substrates *Nanotechnology* **16** 1311–6
[43] Hoo C M, Starostin N, West P and Mecartney M L 2008 A comparison of atomic force microscopy (AFM) and dynamic light scattering (DLS) methods to characterize nanoparticle size distributions *J. Nanopart. Res.* **10** 89–96
[44] Souza T G F, Ciminelli V S T and Mohallem N D S 2015 An assessment of errors in sample preparation and data processing for nanoparticle size analyses by AFM *Mater. Charact.* **109** 198–205
[45] Balnois E, Papastravou G and Wilkinson K J 2007 Force microscopy and force measurements of environmental colloids *Environmental Colloids and Particles: Behaviour, Structure and Characterization* (*IUPAC Series on Analytical*

and Physical Chemistry of Environmental Systems) ed K J Wilkinson and J R Lead (Chichester: Wiley) pp 405–68

[46] Jaskiewicz K, Makowski M, Kappl M, Landfester K and Kroeger A 2012 Mechanical properties of poly (dimethylsiloxane)-block-poly(2-methyloxazoline) polymersomes probed by atomic force microscopy *Langmuir* **28** 12629–36

[47] Habel J *et al* 2015 Selecting analytical tools for characterization of polymersomes in aqueous solution *RSC Adv.* **5** 79924–46

[48] Ramachandran S, Quist A P, Kumar S and Lal R 2006 Cisplatin nanoliposomes for cancer therapy: AFM and fluorescence imaging of cisplatin encapsulation, stability, cellular uptake and toxicity *Langmuir* **22** 8156–62

[49] Rico F, Su C and Scheuring S 2011 Mechanical mapping of single membrane proteins at submolecular resolution *Nano Lett.* **11** 3983–6

[50] Tang E S K, Huang M and Lim L 2003 Ultrasonication of chitosan and chitosan nanoparticles *Int. J. Pharm.* **265** 103–14

[51] Fabregas A, Minarro M, Garcia-Montoya E, Perez-Lozano P, Carrillo C, Sarrate R, Sanchez N, Tico J R and Sune-Negre J M 2013 Impact of physical parameters on particle size and reaction yield when using the ionic gelation method to obtain cationic polymeric chitosan-tripolyphosphate nanoparticles *Int. J. Pharm.* **446** 199–204

[52] Berillo D, Mattiasson B and Kirsebom H 2014 Cryogelation of chitosan using noble-metal ions: *in situ* formation of nanoparticles *Biomacromolecules* **15** 2246−55

[53] Hou D, Gui R, Hu S, Huang Y, Feng Z and Ping Q 2015 Preparation and characterization of novel drug-inserted-montmorillonite chitosan carriers for ocular drug delivery *Adv. Nanoparticles* **4** 70–84

[54] Yongjun L, Zhijin C, Chunxi L, Yu D, Zaijun L and Zhang N 2011 Gadolinium-loaded polymeric nanoparticles modified with Anti-VEGF as multifunctional MRI contrast agents for the diagnosis of liver cancer *Biomaterials* **32** 5167–76

[55] Zhang L, Liu Y, Yu D and Zhang N 2013 Gadolinium-loaded chitosan nanoparticles as magnetic resonance imaging contrast agents for the diagnosis of tumor *J. Biomed. Nanotechnol.* **9** 863–9

[56] Zhang L, Tingxian L, Yanan X, Yu D and Zhang N 2015 Hyaluronic acid-chitosan nanoparticles to deliver Gd DTPA for MR cancer imaging *Nanomaterials* **5** 1379–96

[57] Cullinan S B, Zhang D, Hannink M, Arvisais E, Kaufman R J and Diehl J A 2003 Nrf2 is a direct PERK substrate and effector of PERK-dependent cell survival *Mol. Cell. Biol.* **23** 7198–209

[58] Cullinan S B and Diehl J A 2004 PERK-dependent activation of Nrf-2 contributes to redox homeostasis and cell survival following endoplasmic reticulum stress *J. Biol. Chem.* **279** 20108–17